Parameter Estimation and Optimization of a Loosely Bound Aggregating Pharmaceutical Crystallization Using in Situ Infrared and Laser Backscattering Measurements

Timokleia Togkalidou,[†] Hsien-Hsin Tung,[‡] Yongkui Sun,[‡] Arthur T. Andrews,[‡] and Richard D. Braatz*,[†]

University of Illinois at Urbana-Champaign, 600 South Mathews Avenue, Box C-3, Urbana, Illinois 61801, and Merck & Co., Inc., 126 East Lincoln Avenue, P.O. Box 2000, Rahway, New Jersey 07065

Model-based experimental design and parameter estimation, coupled with in situ infrared and laser backscattering instrumentation, was applied to the cooling crystallization of a drug compound to construct a model for use in the design of an optimal operating procedure. Because the model was constructed completely from in situ sensor data, with no sampling procedures, the amount of pharmaceutical compound required for batch process development was significantly reduced. Modeling issues involving the selection of the expressions for the supersaturation and nucleation rate, as well as the electronics mode in the laser backscattering instrument, were explored. All but one of the kinetic parameters from the gray-box model constructed using laser backscattering data were close to the kinetic parameters for a first-principles model constructed from data from off-line particle size measurements. The model was used to design batch operating procedures to minimize nucleation and maximize the sharpness of the crystal size distribution. This appears to be the first time that the procedure of model-based experimental design, parameter estimation, model selection, and optimization has been applied to the crystallization of a pharmaceutical, as well as the first time that this procedure has been applied to a crystallization process that forms loosely bound aggregates.

1. Introduction

Crystallization is an important purification and isolation step in the production of bulk pharmaceuticals. Batch crystallization is widely used in industry, with a large proportion of the processes being seeded. The crystallization kinetics must be determined experimentally before systematic design of a crystallization process and computation of optimal operating conditions and control procedures can be performed. Current ab initio techniques are unable to determine the kinetics accurately, and thus, the kinetic parameters must be estimated experimentally. Because of the diverse chemical and physical properties of pharmaceutical compounds and the large number of factors that affect crystal product quality [e.g., which are specified in terms of characteristics of the crystal size distribution (CSD), which affects filtration times, flowability, bioavailability, tabletting characteristics, etc.], a combination of trial-and-error testing and empiricism is typically applied. This empirical approach consumes significant resources and time, and the results and conclusions are generally case-specific. Large amounts of resources and experimental time are spent for each compound in order to address the various factors (e.g., seed characteristics, temperature profiles) that can potentially impact the crystallization process. In the pharmaceutical industry, it is highly desirable to bring a crystal product to large-scale production as quickly as possible. It is also essential to be able to design an optimized large-scale process utilizing the smallest amount of materials, as the pharmaceutical is available only in limited quantities during the development of the process.

To minimize the time and resources needed for process development, we explore an alternative to the empirical approach used in pharmaceutical crystallization. We propose the use of model-based experimental design (MBED), parameter estimation, model selection, and process optimization[1−4] implemented on an experimental system in which *all* sensors are in situ. Advantages of developing a model are that (1) models are needed to move pharmaceutical crystallization from an art to a science/engineering task, (2) the iterative process of constructing a model increases process understanding, and (3) models enable a systematic investigation of the effects of different seeding strategies and nonideal mixing through simulations (see ref 5 and references therein). MBED minimizes the number of experiments required to construct a sufficiently accurate model. This is achieved by finding experimental conditions (seed characteristics and supersaturation profile) that optimize the information content of the data. The accuracy of the model parameters is quantified by a confidence hyperellipsoid (the generalization of the confidence interval used in the single-parameter case) whose size is a function of the information content of the data used in the parameter estimation procedure. In parameter estimation, the sum of squared errors between the model predictions and the measured variables is minimized. Both the parameter estimation and MBED procedures are written in terms of optimization problems. This approach is built upon models that utilize the information contained in the large quantity of data collected through in situ infrared and laser backscattering sensors. Because a large amount of data

* To whom correspondence should be addressed. Tel.: 217-333-5073. Fax: 217-333-5052. E-mail: braatz@uiuc.edu.
[†] University of Illinois at Urbana-Champaign.
[‡] Merck & Co., Inc.

10.1021/ie0340847 CCC: $27.50
Published on Web 08/10/2004

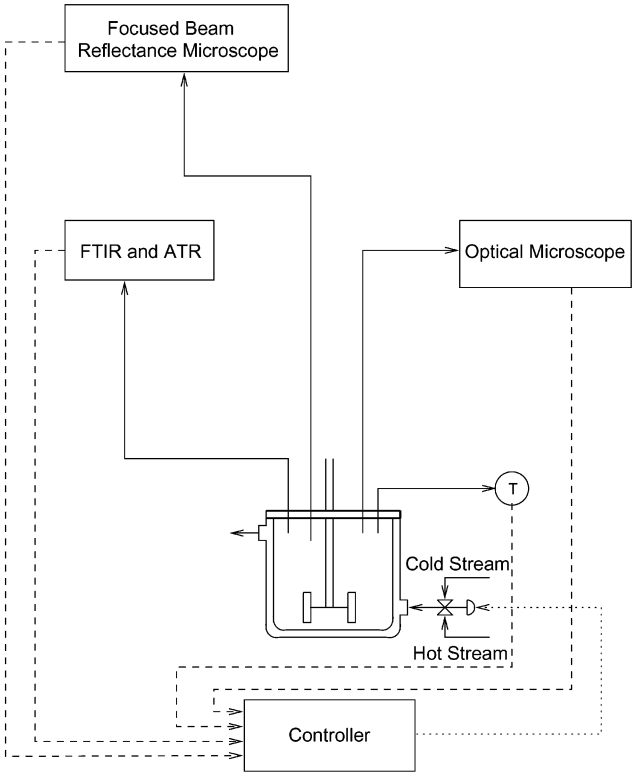

Figure 1. Experimental setup.

is collected and exploited within each batch experiment, this procedure can estimate a crystallization model within a few experiments. Then, the model can be used to predict and optimize the desired crystal product quality by manipulating the seed characteristics and supersaturation profile.

2. Experimental System and Optimization Objective

As shown in Figure 1, the experimental apparatus consisted of a 5-L jacketed crystallizer with an external recirculation loop and three on-line immersion measurement probes. In situ measurements of the infrared spectra were collected using an ASI Applied System ReactIR 1000 FTIR spectrophotometer with an attenuated total reflection (ATR) immersion probe. The FTIR spectra were collected in the range 650−4000 cm^{-1}. The infrared spectra were related to the solute concentration using robust chemometrics.[6] Chord length distribution (CLD) measurements were collected every 2 min using a Lasentec focused-beam reflectance measurement (FBRM, model D600L) instrument, where the *chord* of a particle is defined as the distance across a particle as observed by optics collecting backscattered light from a laser crossing the particle. In addition, in situ images of the slurry were acquired using a Lasentec particle vision microscopy (PVM, model 700L) instrument. The batch vessel was equipped with an overhead four-pitched-blade agitator. The temperature was controlled using a HAAKE C50 water/glycol temperature bath and was measured using a temperature probe attached to the FTIR spectrophotometer.

A typical crystallization procedure follows: The crystallizer was charged with appropriate amounts of toluene and a Cox-2-specific inhibitor drug candidate. Both milled and unmilled seeds were available for use. After charging, the batch temperature was raised to 60 °C so that all crystals dissolved. The temperature was kept at 60 ° for 1 h to ensure that no crystals were present. Then, the temperature was reduced to 50 °C. The crystallizer was seeded with appropriate amounts of milled or unmilled seed. Then, the batch was cooled to 20 °C over a specific amount of time. The experimental conditions and constraints used in the study are listed in Table 1.

In this study, the objective was to select seed characteristics and a temperature profile that optimized a characteristic property of the product crystals while satisfying constraints on the cooling rate, quantity of seed crystals, duration of crystallization, and yield. The subsequent sections describe the crystallization model, sensor technologies, the model-building and optimization approach, and results and discussion.

3. Crystallization Model

It was assumed that the crystallizer was well-mixed, that is, there were no spatial variations of the states of the crystallizer (temperature, solute concentration, and crystal size distribution). It was also assumed that the crystallization procedure was dominated by nucleation and growth phenomena (an assumption regarding aggregation will be discussed later). The growth rate of crystals was assumed to be independent of size. Such assumptions are common in the industrial crystallization literature.[7] The population balance for a batch crystallizer is[8]

$$\frac{\partial f(L,t)}{\partial t} + G(S;\theta_g)\frac{\partial f(L,t)}{\partial L} = B(S,f;\theta_b)\,\delta(L - L_0) \quad (1)$$

where $f(L,t)$ is the population density function, $G(S;\theta_g)$

Table 1. Experimental Conditions and Constraints

variable	name	value	units
$m_{solvent}$	mass of solvent	3800	g
ρ_c	crystal density	1.41	g/cm^3
L_0	nucleated crystal size	0[a]	μm
C_0	initial concentration	0.197	g of solute/g of solvent
C_{sat}	saturation concentration	$0.0845T^2 + 2.3547T + 64.224$	g of solute/g of solvent
k_v	volumetric shape factor	1.8	
T_{max}	maximum T constraint	50	°C
T_{min}	minimum T constraint	20	°C
R_{max}	maximum temperature gradient	0, 15, 20	°C/h
R_{min}	minimum temperature gradient	−15, −20	°C/h
$m_{seed,max}$	maximum seed mass as a percentage of the total mass in solution	6%	g
$m_{seed,min}$	minimum seed mass as a percentage of the total mass in solution	1%	g

[a] Essentially the same results are obtained with L_0 set to a realistic nonzero value.

is the growth rate of the crystal along the characteristic dimension, $B(S,f;\theta_b)$ is the nucleation rate of crystals, θ_g and θ_b are sets of growth and nucleation parameters, L is the characteristic dimension, $L_0 > 0$ is the characteristic size for nucleating crystals, S is the supersaturation, and $\delta(\cdot)$ is the delta function. The initial condition for the population balance is given by the population density function of the seed crystals $f(L,0) = f_0(L)$. Assuming that there is no mechanism of producing crystals of size $L_0 = 0$ and that the initial distribution does not have crystals of size $L = 0$, the boundary condition is $f(0,t) = 0$, $\forall t \in [0, \infty)$.

The two common expressions for supersaturation used in the literature are the relative supersaturation $S = (C - C_{sat})/C_{sat}$ and the absolute supersaturation $S = C - C_{sat}$. The population balance equation can be converted into the following set of differential equations by multiplying both sides of eq 1 by L^j for $j = 0, 1, 2, ...$, and integrating each term from 0 to ∞[9]

$$\frac{d\mu_0}{dt} = B$$

$$\frac{d\mu_j}{dt} = jG\mu_{j-1} + BL_0^j, \quad j = 1, 2, ... \tag{2}$$

where the jth moment is defined as

$$\mu_j \equiv \int_0^\infty L^j f(L,t)\, dL \tag{3}$$

and the population density function is in units of particle number per unit length per unit solvent mass. The product quality objectives (described in section 5) are computed from μ_0 to μ_3. The moment μ_4 was also simulated because it was used to compare model predictions to FBRM data.

A separate set of differential equations was solved for the seed crystals[4]

$$\frac{d\mu_0'}{dt} = 0$$

$$\frac{d\mu_j'}{dt} = jG\mu_{j-1}', \quad j = 1, 2, ... \tag{4}$$

where μ_j' represents the moments of the seed crystals. Thus, one set of equations (eqs 2) tracks the moments of all crystals in the slurry (both nucleated and seed crystals), and the other set (eqs 4) tracks the moments of the crystals grown from the initial seed crystals. The separate set of equations for the seed crystals allows for the computation of the ratio of the crystal mass grown from nuclei to the crystal mass grown from seed, which quantifies the total amount of nucleation occurring in the crystallizer.[3,4] Minimizing the nucleated-to-seed mass ratio is consistent with the commonly used design objective of minimizing the total amount of nucleation that occurs during the batch run.[10] The initial conditions necessary to solve the set of equations both for μ_j and μ_j' are given by the moments of the seed crystals. The initial moments of the seed crystals are calculated from the FBRM measurements immediately after seeding. The usual simplification is made that the nucleated crystals are of negligible size ($L_0 = 0$).[7,9] Inserting realistic nonzero values for L_0 gives essentially the same moments and solute concentration predictions, because the terms that contain L_0 in the moment equations (e.g., in the second line of eqs 2) are many orders of magnitude smaller than the rest of the terms in the equations. The nucleation term appears in the equation for the zeroth moment (i.e., see the first line of eqs 2), which affects the rest of the ODEs as they are directly or indirectly dependent on the zeroth moment.

The solute mass balance is[4]

$$\frac{dC}{dt} = -\rho_c k_v (3G\mu_2 + BL_0^3) \tag{5}$$

where C is the solute concentration in units of mass of solute per unit mass of solvent, ρ_c is the crystal density, and k_v is the volumetric shape factor. The initial condition for the solute concentration is its value at the seeding point. For the case where the crystals are modeled as having two independent growth axes, two-dimensional moments of the crystals are used[8,11]

$$\mu_{ij} \equiv \int_0^\infty \int_0^\infty L_1^i L_2^j f(L_1,L_2,t)\, dL_1\, dL_2 \tag{6}$$

and the corresponding set of moment equations are

$$\frac{d\mu_{00}}{dt} = B$$

$$\frac{d\mu_{ij}}{dt} = iG_1\mu_{(i-1)j} + jG_2\mu_{i(j-1)} + BL_{01}^i L_{02}^j, \quad i + j > 0 \tag{7}$$

where L_{01} and L_{02} are the characteristic width and length of nucleating crystals and G_1 and G_2 are the growth rates along each of the characteristic dimensions.

Various expressions for the growth rate kinetics have been proposed.[9,12] Most of these mechanisms predict that the growth rate is independent of crystal size, an idea that is attributed to McCabe and is termed the ΔL law. This study assumes a size-independent growth rate $G = k_g S^g$, where k_g and g are kinetic parameters to be estimated, as has been observed in a large number of systems in the literature.[7,9] The parameter g can be between the values of 1 and 2 depending on the rate-limiting steps in the crystal growth mechanism.[9] This study also makes the common assumption that the temperature dependence of the kinetic parameters is negligible.[7,9] The same moments methodology can be employed for crystal growth rates that depend affinely on size,[8,9] and the same parameter estimation approach applies to systems with a significant temperature dependence of the growth rate. For crystallization in which there are two independent growth dimensions, the growth rate kinetics are described by $G_1 = k_{g1} S^{g_1}$ and $G_2 = k_{g2} S^{g_2}$ along the two characteristic dimensions.

In general, nucleation is classified into two categories, primary or secondary, for nucleation in the absence and in the presence of crystals, respectively. Here, secondary nucleation from crystal surfaces is considered, because it is the dominant mechanism in most seeded crystallizers. The two most common expressions for the secondary nucleation rate are $B = k_b S^b \mu_2$ and $B = k_b S^b \mu_3$, where k_b and b are nucleation parameters to be estimated.[9] The parameter b is usually observed experimentally to be between 1 and 3.[9] An expression for the nucleation rate for the two-dimensional case is $B = k_b S^b \mu_{2,1}$, given that L_1 is the smallest characteristic dimension.[11]

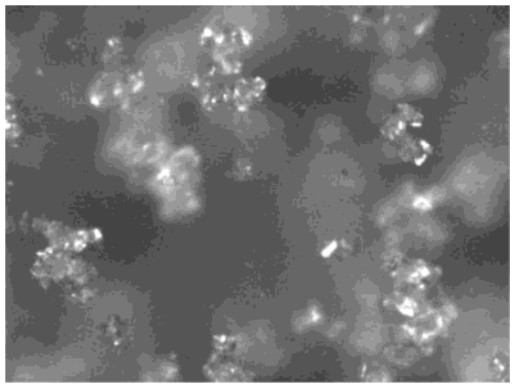

Figure 2. PVM image of slurry taken in-process during batch crystallization.

The pharmaceutical under investigation forms loosely bound aggregates, as shown in the in situ image taken using PVM (see Figure 2). According to manufacturer documentation from Lasentec,[13] for sufficiently loosely bound aggregates, the FBRM instrument predominantly measures the chords of the individual crystals in the aggregates, rather than chords across the entire aggregates. This assertion was supported by the observation that the average size of the individual crystals measured using the FBRM instrument was within measurement variations of the average size of the individual crystals observed using the PVM instrument. Off-line optical microscopy images also supported this hypothesis. A sample of product slurry was collected at the end of a batch, filtered, and measured under an optical microscope. The average and maximum sizes of the individual particles in the product aggregates were within measurement variations of the average and maximum chords measured by FBRM. In contrast, the average and maximum sizes of the product aggregates were much larger (approximately a factor of 5) than the average and maximum chords measured by FBRM. A more detailed comparison of the FBRM data with the size of individual crystals in the aggregates is given in section 6.

The aforementioned equations for the population density function (eq 1) and the moment equations can be applied to an aggregating system, provided that the population density is defined for *the individual crystals in the aggregates*. In contrast, additional integral aggregation terms would need to be included in eq 1 if the population density function *of the aggregates* were being modeled.[9] This focus on the modeling of the individual crystals greatly simplifies the modeling of the system. This simplification is necessary if a model is to be developed from a small number of experiments using existing in situ sensors, as there are no in situ sensors on the market that can measure the number of individual particles in loosely bound aggregates and accurately measure the mass or size of such aggregates. Without this information, it is not possible to identify the integral terms used to model aggregation (in contrast, it is possible to identify the aggregation kernels in a simplified laboratory system if the aggregates/agglomerates are bound tightly enough to be roughly spherical[9]). Therefore, the approach taken here provides no information on the number of individual crystals in or the size or mass of the aggregates. Also, this approach should be considered only for loosely bound aggregates, in which the individual crystals retain most of their external surface area, without significant surface area being "covered up" by adjoining particles.

As in the modeling of any reasonably complex system, various assumptions are made that have various degrees of accuracy. For example, some crystallizations have size-dependent growth kinetics and/or growth dispersion.[9,14] Some crystals have an inherent growth rate depending on the origin of their nuclei, where crystals with a greater number of initial dislocations will grow faster. The predictive ability of the model and the magnitude of the confidence intervals on the kinetic parameters (whose computation is discussed in section 5) are used to determine whether the assumed kinetic expressions, as well as other model assumptions, are consistent with the experimental observations. Large confidence intervals on the kinetic parameters, that persist after several batch experiments have been conducted, would suggest that poor assumptions had been made in the model.[15]

4. Sensor Technologies and Gray-Box Modeling

In situ or "in-process" sensors do not require sampling of the crystal slurry during the crystallization process. This reduces the amount of pharmaceutical needed for each batch experiment, which is an important consideration when a limited amount of pharmaceutical is available during the early stages of process development. The trend in the pharmaceutical industry is to move to smaller crystallizers for early-stage studies, increasing the effects of sampling on the crystallizer. Also, sampling always affects the sample itself, so that it is not completely representative of the bulk slurry.

For this study, FTIR spectral data were used to infer the solute concentration,[6] and FBRM data provided size information throughout the batch. Inferential modeling was used to construct a calibration curve to relate the FTIR spectra to the solute concentration, using procedures described elsewhere.[16−18] The calibration curves are determined off-line, using a small number of samples.

FBRM measures the CLD, which is not the same as the crystal size distribution (CSD),[19] although the moments of the CLD can be correlated to important downstream process characteristics. For example, it has been shown that various moments of the CLD are correlated with the filtration resistance and the filtration time of the slurry[16] and that chord length measurements of aggregates in suspension correlate with rheological behavior (the yield stress) of the suspension.[20] In a pulp and paper application,[21] the FBRM technique was used for wet-end optimization at an uncoated woodfree paper mill and web break prediction at a corrugated board mill.

The particle size distribution (PSD) can be computed from the CLD, under certain assumptions including that the particle shape is known.[19,22] There are several methods for estimating the PSD from the CLD for spherical particles.[23,24] The effect of the surface roughness can be taken into account, which can be an important consideration for particles with surface irregularities.[23] For other systems, the square-weighted chord length was found to be comparable to laser diffraction, sieving, and electrical sensing zone analysis over the range of 50−400 μm.[25]

Although the aforementioned methods have successfully estimated the PSD from the CLD for some systems, the theory behind these methods require many assumptions, including that the particles perfectly backscatter

light at all angles and that all particles have a known shape. Although these assumptions are true for many particulate systems (such as round polymer beads with a rough surface in water at low-to-moderate solids densities[23]), the assumptions are not accurate for other particulate systems (such as droplets that have poor backscattering properties). For some systems, unmodeled factors such as the optical properties of solids and solvents, as well as positioning of the probe in relation to the surrounding flow, can significantly affect the CLD,[22] which, in turn, significantly affects the estimated PSD. The time and the available quantity of pharmaceutical compound are typically quite limited in the early-stage design of the batch crystallization process, which limits the ability to carry out the investigative studies needed to verify the assumptions and to determine the effects of nonideality of the assumptions on the accuracy of the estimates of the PSD from the CLD. Also, the proper technique for computing the PSD from the CLD when the underlying assumptions of the methods do not hold is still an open problem.

An alternative approach applicable in the early-stage design of pharmaceutical crystallization processes is to use the low-order moments of the CLD directly, without first converting the CLD measurement to a PSD estimate. This approach replaces the first-principles model for the PSD with a *gray-box* model for the CLD, in which the structure of the first-principles model for the low-order moments of the PSD is used to parametrize the low-order moments for the CLD. Gray-box modeling is in contrast to black-box modeling approaches such as finite impulse response and dynamic artificial neural network models, which typically ignore first principles in their parametrization of the process dynamics. Gray-box models are commonly used in process control, as they have lower data requirements and some of the improved extrapolation capability of first-principles models without requiring all of the information needed to construct a first-principles model.[26] The reasoning behind this particular gray-box model is that the mapping between the CLD and the PSD is static (most of the aforementioned mapping methods assume that the mapping is actually linear), so the low-order moments of the CLD should follow the same *dynamic* trends as the low-order moments of the PSD. As with any model, its applicability is assessed by quantifying the accuracy of the kinetic parameters and its predictions (as discussed in ref 15 and references therein). If the gray-box model is a poor parametrization of the low-order moments of the CSD, then it will be impossible to obtain small confidence intervals on the kinetic parameters because of model bias errors. If the gray-box model is a good parametrization, then it will be possible to obtain small confidence intervals on the kinetic parameters and good predictions (see, for example, eq 5.8.12 of ref 15 and the associated discussion).

5. Background on Model Building and Optimization

The overall procedure consists of model-based experimental design (MBED),[27−29] inferential modeling, parameter estimation,[15,30−33] model selection, and optimization as the fundamental tasks. MBED and parameter estimation are repeated until the parameter estimates are sufficiently accurate. These kinetic parameters are incorporated into a model and used to design a batch operating procedure that optimizes product quality.

For the design of the first experiment, the user provides an initial guess of the kinetic parameters. If no such parameters are available, the user can follow the existing crystallization procedure as the first experiment, provided that this experiment exhibits sufficient dynamic behavior. The kinetic parameters are estimated from the measurements of the solute concentration and moments by minimizing the differences between the model predictions and measurements[28,34]

$$\min_{\theta} \sum_{i=1}^{N_m} \sum_{j=1}^{N_d} w_{ij} [y_{ij}^{meas} - y_{ij}^{model}(\theta)]^2 \qquad (8)$$

where θ is the set of the parameters to be estimated, y_{ij}^{meas} represents the measurements, y_{ij}^{model} represents the model predictions, N_m is the number of measured variables, N_d is the number of sampling instances, and w_{ij} is a weighting factor. Under mild assumptions, the best value for w_{ij} is the inverse of an estimate of the error variance σ_i^2, where σ_i is the standard deviation for the error in the ith measurement. The error variances are typically selected to account for deviations due to measurement inaccuracies and small levels of model inadequacy (e.g., see page 181 of ref 15). For the first parameter estimation, σ_i is set to the standard deviation of the actual measurement. A set of parameters was estimated by solving the optimization problem in eq 8, and the standard deviation σ_i for the error in the ith measurement was also estimated for each measurement. These new values of standard deviation σ_i for the error in the ith measurement were fed to the parameter estimation problem and the optimization problem was solved again. The iterative procedure was repeated until no significant difference between the given and estimated standard deviations was detected.

Confidence intervals for each parameter were computed. Briefly, the approximate $100(1 - \alpha)\%$ confidence region is the hyperellipsoid defined by

$$(\theta - \theta^*)^T V_\theta^{-1} (\theta - \theta^*) = \chi_{N_p}^2(\alpha) \qquad (9)$$

where V_θ is the parameter covariance matrix, θ is the true value of the parameter (unknown), θ^* is the estimate of the parameter, $\chi_{N_p}^2$ is the chi-squared distribution with N_p degrees of freedom, and N_p is the number of parameters. Estimates of the confidence intervals are computed from the diagonal elements of the parameter covariance matrix.[15] Once the parameters and confidence intervals have been estimated, a decision is made as to whether the accuracy of the parameters is adequate. If the confidence intervals on the parameters are large, the user proceeds to MBED, which is posed as an optimization problem[7,15,35,36]

$$\min\{\text{volume of confidence ellipsoid}\} = \max[\det(V_\theta^{-1})] \qquad (10)$$

subject to the constraints on the experimental procedure (see Table 1) and the crystallization model described in section 3. This optimization computes experimental conditions to minimize the volume of the confidence ellipsoid on the parameters, which is inversely proportional to the determinant of V_θ^{-1}.[27] The optimization problem was solved by sequential quadratic programming,[37,38] with the temperature profile parametrized by a finite number of linear segments.

In this study, the experimental design variables were the temperature profile and seed load, with the seed distribution modeled by a quadratic function. The lower bound of seed load of 3% was selected on the basis of current operations. Very small seed loads lead to operations problems, in which fluctuations in temperature or shifts in the solubility curve can cause all of the seed crystals to dissolve, leading to uncontrolled nucleation as the crystallizer temperature decreases. An upper bound of 6% for the seed load was selected because of the limited availability of the crystals. The constraints reported in Table 1 are associated with the characteristics of the crystallizer (such as temperature and temperature gradient constraints) and with the available resources (such as the mass and size distribution of seed crystals and the duration of experiment). The reader is referred to the refs 3, 7, 35, and 36 for more details on the application of MBED to crystallization processes.

This iterative procedure of MBED, batch experimental data collection, and parameter estimation is repeated until the parameters are sufficiently accurate. Because a significant quantity of informative data is collected and exploited in each batch experiment, a small number of experiments is typically sufficient for an accurate model to be constructed. This model is used to optimize a characteristic property associated with the product quality over the temperature profile and seed mass

$$\min_{\text{seed,temperature}} (\text{crystal property}) \qquad (11)$$

subject to the operating constraints of the crystallization. For this study, the crystal properties that were optimized were the coefficient of variation (cov) and the nucleated-to-seed mass ratio. The cov was computed as $\sqrt{\mu_2\mu_0/\mu_1^2-1}$, which gives a measure of the spread of the distribution about the mean. The nucleated-to-seed mass ratio is defined as the ratio of crystal mass grown from nucleated crystals to the crystal mass grown from seed crystals, which can be computed from the moments model. The operating constraints were associated with economics (a lower bound on the yield and an upper bound on the seed mass and duration of crystallization), the characteristics of the crystallizer (upper and lower bounds on the temperature and temperature gradient and a lower bound on the seed mass), and available materials (the seed distributions that were available), with the constraints in this study reported in Table 1. The optimization problem in eq 11 including the model and operating constraints was solved by applying sequential quadratic programming to the simulation code, which was implemented using the sparse solver LSODES.

6. Results and Discussion

The goal of MBED is to improve the effectiveness of efforts to construct an accurate model from a minimal number of experiments. Because no prior knowledge of the growth and nucleation parameters was available, the first experiment (experiment 1a in Table 2) followed the existing procedure. The resulting experimental data were used to select the supersaturation expression, by comparing the confidence intervals on the kinetic parameters obtained in the various models. A hardware mode (coarse vs fine electronics) in the FBRM was selected by comparing confidence intervals between the data from experiments 1a and 1b (see Table 2), which uses the same experimental conditions as experiment 1a but a different electronics mode. The data from experiment 1a and the associated kinetic parameter estimates from the selected model were used to design the temperature profile and the seed load in experiment 2 using MBED. The data from experiments 1a and 2 were used to select the moment order in the nucleation expression, with the best model having kinetic parameters with an accuracy of 12%. A fourth *independent* experiment (experiment E) was used with off-line optical microscopy to evaluate the accuracy of (i) the FBRM technique in measuring the low-order moments of the individual crystals, (ii) the kinetic parameters obtained using the FBRM data, and (iii) the predictions of the model obtained using the FBRM data. A final experiment (experiment 3) was conducted using the operating procedure designed to optimize a crystal product property of interest. Table 2 summarizes the operating conditions for the experiments. Table 3 lists the initial moments for each experiment calculated by the FBRM signal immediately after seeding.

Table 2. Experiments, Seed Loads, Cooling Profiles, and FBRM Electronics

expt	seed level	cooling profile	Lasentec FBRM electronics
1a	milled seed, 3%	see Figure 9, expt 1a	fine
1b	milled seed, 3%	see Figure 9, expt 1a	coarse
2	unmilled seed, 3%	see Figure 9, expt 2	fine
E	milled seed, 3%	see Figure 7	fine
3	milled seed, 6%	see Figure 9, expt 3	fine

Table 3. Initial Moments for Experiments 1a, 1b, 2, and 3

expt	μ_0	μ_1	μ_2	μ_3	μ_4
1a	3.35×10^5	8.64×10^6	3.51×10^8	1.92×10^{10}	1.33×10^{12}
1b	9.63×10^4	4.33×10^6	2.76×10^8	2.32×10^{10}	2.42×10^{12}
2	1.55×10^5	3.89×10^6	1.58×10^8	8.73×10^9	6.41×10^{11}
3	5.70×10^5	1.19×10^7	4.07×10^8	1.91×10^{10}	1.14×10^{12}

6.1. Hardware Mode. The manufacturer documentation for the FBRM instrument indicates that the coarse electronics mode filters the backscattering light signal before measuring chords, whereas the fine mode uses an unfiltered signal that is more likely to measure the individual crystals within loosely bound aggregates.[13] Parameters and their confidence intervals for experiments 1a and 1b (in which fine and coarse modes, respectively, were used) are listed in Table 4. The confidence intervals obtained using the fine electronics were smaller than those obtained using coarse electronics. The predicted and measured values for the solute concentration and the low-order moments are reported for experiment 1a in Figure 3 and for experiment 1b in Figure 4. For experiment 1a, the predicted values agree well with the measured values for the first, second, and third moments, whereas poorer agreement is observed for the solute concentration and the zeroth and fourth moments. For experiment 1b, fairly good agreement is established for the second and third moments, whereas poor agreement is observed for the solution concentration and the zeroth, first, and fourth moments. The fine electronics mode was used in subsequent experiments because of its smaller confidence intervals and better tracking of the variables. Selecting the fine mode as the device setting is consistent with the assumption in the model that the low-order moments of the CLD are for the individual crystals in the agglomerates. Further evaluation of the measurement device is provided in section 6.5.

Table 4. Nucleation and Growth Kinetic Parameters and Confidence Intervals for Fine and Coarse Electronics and the Two Supersaturation Expressions with the $B = k_b S^b \mu_3$ Nucleation Model

electronics	S	g	$\ln(k_g)^a$	b	$\ln(k_b)^b$
fine	$S = C - C_{sat}$	2.00 ± 0.45 $\pm 22.5\%$	-6.81 ± 1.28 $\pm 18.9\%$	1.07 ± 0.24 $\pm 22\%$	10.63 ± 0.68 $\pm 6.4\%$
coarse	$S = C - C_{sat}$	1.37 ± 0.38 $\pm 27\%$	-4.41 ± 1.13 $\pm 26\%$	1.42 ± 0.46 $\pm 32\%$	8.53 ± 1.33 $\pm 15\%$
fine	$S = (C - C_{sat})/C_{sat}$	1.09 ± 0.43 $\pm 39\%$	1.70 ± 1.02 $\pm 60\%$	1.05 ± 0.48 $\pm 45.7\%$	16.61 ± 1.18 $\pm 7.1\%$

[a] Dimensions for k_g are (cm/min)(kg of solvent/g of solute)^g for absolute supersaturation and cm/min for relative superaturation. [b] Dimensions for k_b are (number of particles/min·cm^3)(kg of solvent/g of solute)^b for absolute supersaturation and (number of particles)/min·cm^3 for relative superaturation.

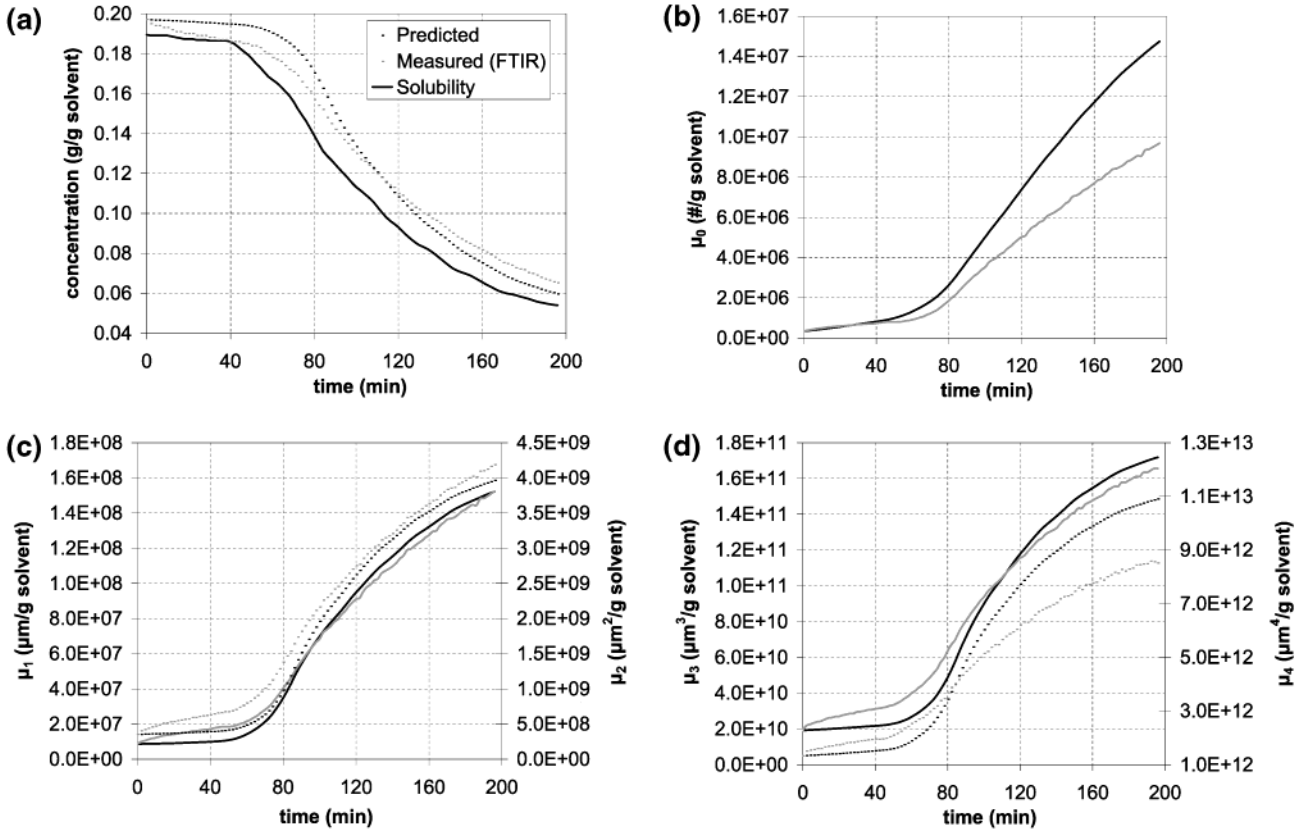

Figure 3. Predicted (black) and measured (gray) variables for experiment 1a: (a) solute concentration; (b) zeroth moment, μ_0; (c) first moment (solid), μ_1, and second moment (dashed), μ_2; (d) third moment (solid), μ_3, and fourth moment (dashed), μ_4.

6.2. Supersaturation Expression. Results from comparing two sets of nucleation and growth expressions are presented here. Using the data from experiment 1a, the absolute supersaturation gave significantly smaller prediction intervals than the relative supersaturation (see Table 4). That the growth rate is a quadratic function of the absolute supersaturation suggests that diffusion through the liquid phase to the crystal surface is not the rate-limiting step for growth.[39] Although the nucleation exponent is on the small side (the usually observed range for secondary nucleation is $1-3$[9]), other researchers have reported similarly small values for some crystallization systems.[7]

6.3. Design of Experiment 2 and Parameter Estimation Results. Once it was decided to use the absolute supersaturation expression and the fine electronics mode for the FBRM instrument, MBED was used to design the temperature profile and seed load for the next experiment, experiment 2. MBED produced a seed load of minimum size (3%, see Table 2). The same result occurred in a parametric study of an inorganic system.[2] The small seed load leads to a higher supersaturation over the batch experiment, resulting in an increase in the nucleation and growth rates, which produces data that contain more information about the nucleation and growth kinetics. As shown in Table 5, experiment 2 resulted in a reduction in the confidence intervals by a factor of 2.

The predicted and measured solute concentration and the low-order moments are reported for experiment 1a in Figure 3 and experiment 2 in Figure 5. For both experiments, close agreement occurs in the first, second, and third moments. Experiment 2 exhibits much better agreement for the solute concentration and fourth moment than experiment 1a. As the level of accuracy of 12% in the kinetic parameters was high enough for the model to be used to optimize the process, resource and time limitations prevented justifying further experiments for use in modeling.

6.4. Expression for the Nucleation Kinetics. The estimates for the kinetic parameters are reported in Table 5 for the case where the alternative nucleation kinetics expression $B = k_b S^b \mu_2$ was used. The widths of the confidence intervals obtained after experiment 2 are

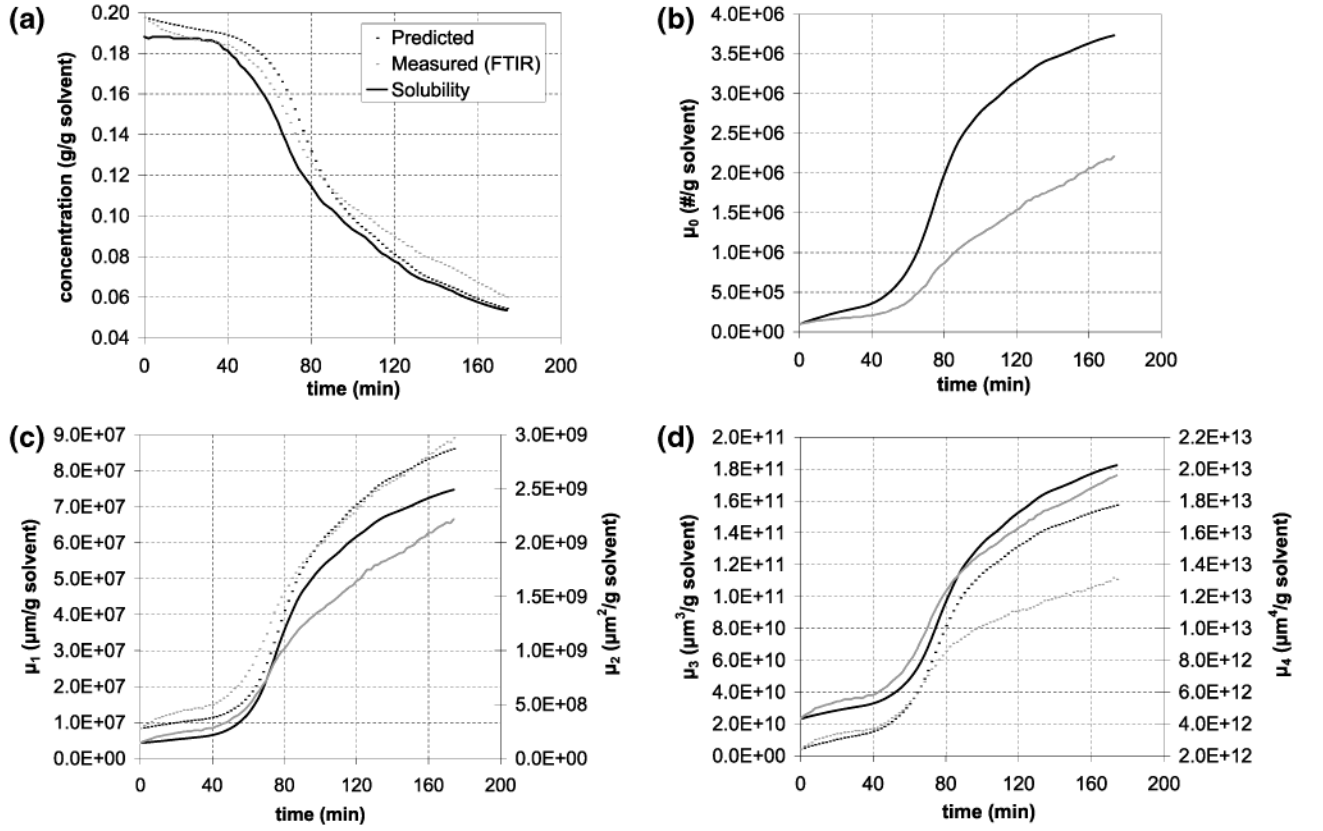

Figure 4. Predicted (black) and measured (gray) variables for experiment 1b: (a) solute concentration; (b) zeroth moment, μ_0; (c) first moment (solid), μ_1, and second moment (dashed), μ_2; (d) third moment (solid), μ_3, and fourth moment (dashed), μ_4.

Table 5. Nucleation and Growth Kinetic Parameters and Prediction Intervals for Two Experiments for the $B = k_b S^b \mu_3$ and $B = k_b S^b \mu_2$ Nucleation Models with Absolute Supersaturation

expt	g	$\ln(k_g)$	B	b	$\ln(k_b)^a$
1a	2.00 ± 0.45 ±22.5%	-6.81 ± 1.28 ±18.9%	$B = k_b S^b \mu_3$	1.07 ± 0.24 ±22%	10.63 ± 0.68 ±6.4%
2[b]	2.00 ± 0.18 ±9%	-6.93 ± 0.59 ±8.5%	$B = k_b S^b \mu_3$	1.00 ± 0.12 ±12%	11.25 ± 0.36 ±3.2%
1a	2.00 ± 0.60 ±30%	-6.47 ± 1.64 ±25.3%	$B = k_b S^b \mu_2$	1.21 ± 0.61 ±50.4%	14.75 ± 1.56 ±11%
2[b]	2.00 ± 0.22 ±11%	-6.50 ± 0.67 ±10.3%	$B = k_b S^b \mu_2$	1.21 ± 0.15 ±12.4%	14.74 ± 0.42 ±3%

[a] Dimensions for k_g in the $B = k_b S^b \mu_2$ model are (number of particles/min·cm^2)(kg of solvent/g of solute)^b(10^4). [b] The second experiment was designed with MBED.

similar to those obtained in the case where the expression $B = k_b S^b \mu_3$ was used. These results are consistent with past studies,[4,35] which also found that it was difficult to distinguish between the two nucleation models from a limited number of batch experiments.

6.5. Sensor and Model Evaluation and Kinetic Parameters for the Two-Dimensional Model. An additional experiment E was conducted in which five samples were removed from the crystallizer during the crystallization process, to be examined under the microscope. This experiment was used to evaluate the predictive ability of the kinetic models for an operating procedure very different from that used to fit the kinetic parameters, as well as to evaluate the level of agreement between low-order moments determined by FBRM and by off-line optical microscopy.

The samples were quickly filtered and sonicated so that any aggregates were separated into individual crystals. Images were taken with a camera connected to an optical microscope (see Figure 6) and analyzed with image analysis software to extract the sizes of the crystals. The number of crystals used to build the population density function for each of the samples ranged between 1000 and 3000 crystals. The kinetic parameters in the two-dimensional crystallization model were fit to the two-dimensional data to estimate the kinetic parameters, which are reported in Table 6. The confidence intervals for the two-dimensional model were estimated using the Monte Carlo method.[15]

Except for the nucleation preexponential parameter, the gray-box model constructed from low-order moments from the CLD gave kinetic parameters very similar to those obtained with as the model constructed from two-dimensional moments measured using off-line optical microscopy (compare Table 5 with Table 6). It is not surprising that a second growth coordinate was unnecessary, as the kinetic growth parameters were not significantly different along the length and width directions. This is consistent with direct examination of the experimental data, where it is observed that the average aspect ratio varies little during the experiments (1.75 for seed crystals, increasing to 1.85 for the product crystals). What is more interesting is that the kinetic parameters determined from low-order moments of the CLD are very similar to the kinetic parameters determined from the CSD measured off-line. As discussed in section 4, the CLD should track the same dynamics as the CSD, as the theoretical mappings between the two are static. It is not much of a leap to suggest that this static relationship is why almost all of the kinetic parameters obtained from the two methods of particle size measurement are very similar. A possible cause for the smaller nucleation preexponential parameter ob-

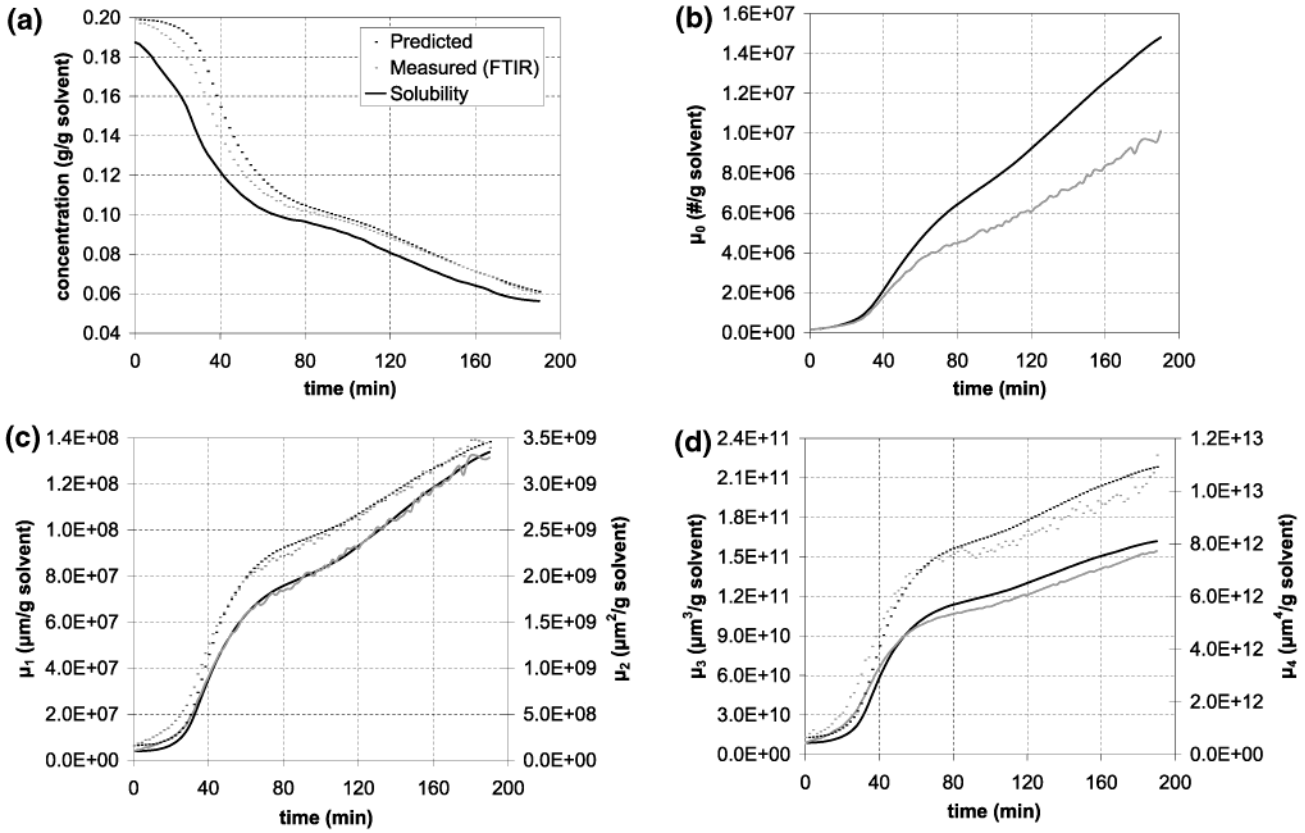

Figure 5. Predicted (black) and measured (gray) variables for experiment 2: (a) solute concentration; (b) zeroth moment, μ_0; (c) first moment (solid), μ_1, and second moment (dashed), μ_2; (d) third moment (solid), μ_3, and fourth moment (dashed), μ_4.

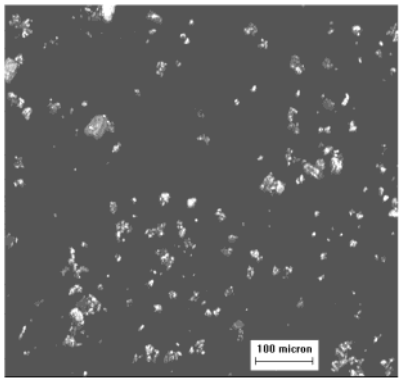

Figure 6. Representative microscope image of crystals from experiment E.

Table 6. Nucleation and Growth Kinetic Parameters for the Two-Dimensional Model

parameter	value	confidence interval
g_1	1.96 ± 0.25	±13%
$\ln(k_{g_1})$	-6.47 ± 0.93	±14%
g_2	1.95 ± 0.29	±15%
$\ln(k_{g_2})$	-6.55 ± 0.96	±15%
b	1.00 ± 0.01	±1%
$\ln(k_b)$	9.51 ± 0.53	±6%

tained from off-line optical microscopy is that the small temperature fluctuations occurring during sampling might have been large enough to dissolve small crystals in the sample, thereby reducing the measured number of crystals. Another possibility is that the sample removed from the crystallizer might not have been representative of the average crystal size distribution in the crystallizer. Such sampling effects are always an issue with sampling-based methods for particle size measurements. These effects can be smaller for in situ probes that are well placed in the crystallizer.

The predicted and measured solute concentration and low-order moments for experiment E are reported in Figure 7. The predicted first, second, and third moments are quite close to the measured values. Poorer prediction was observed for the zeroth and fourth moments. Overall, the prediction of the moments should be considered as being very good. Obtaining a more accurate prediction of the zeroth moment should not be expected, considering that this moment is proportional to the number of crystals and the smallest crystals (less than $\sim$0.5 μm) cannot be observed by the FBRM instrument. Obtaining a more accurate prediction of the fourth moment should not be expected, given that the L^4 term in its integral magnifies the effects of counting small numbers of large particles, which can be biased downward by the FBRM instrument because of the undercounting of the small numbers of large particles as only a finite number of particles being counted. The poor prediction of the solute concentration could be due to experiment E having a temperature profile that was very different from the experiments used to fit the parameters in the model (experiments 1a and 2) or to a bias or slow drift in the concentration measurements for that experiment.

The moment ratios measured by FBRM, predicted by the one-dimensional model, and measured using off-line optical microscopy are reported in Tables 7 and 8. Significant differences in some of the variables were observed immediately after the seed point, with most of the differences becoming smaller as the crystallization progressed. The average size from the one-dimensional model (μ_1/μ_0) was bounded or nearly bounded for all of

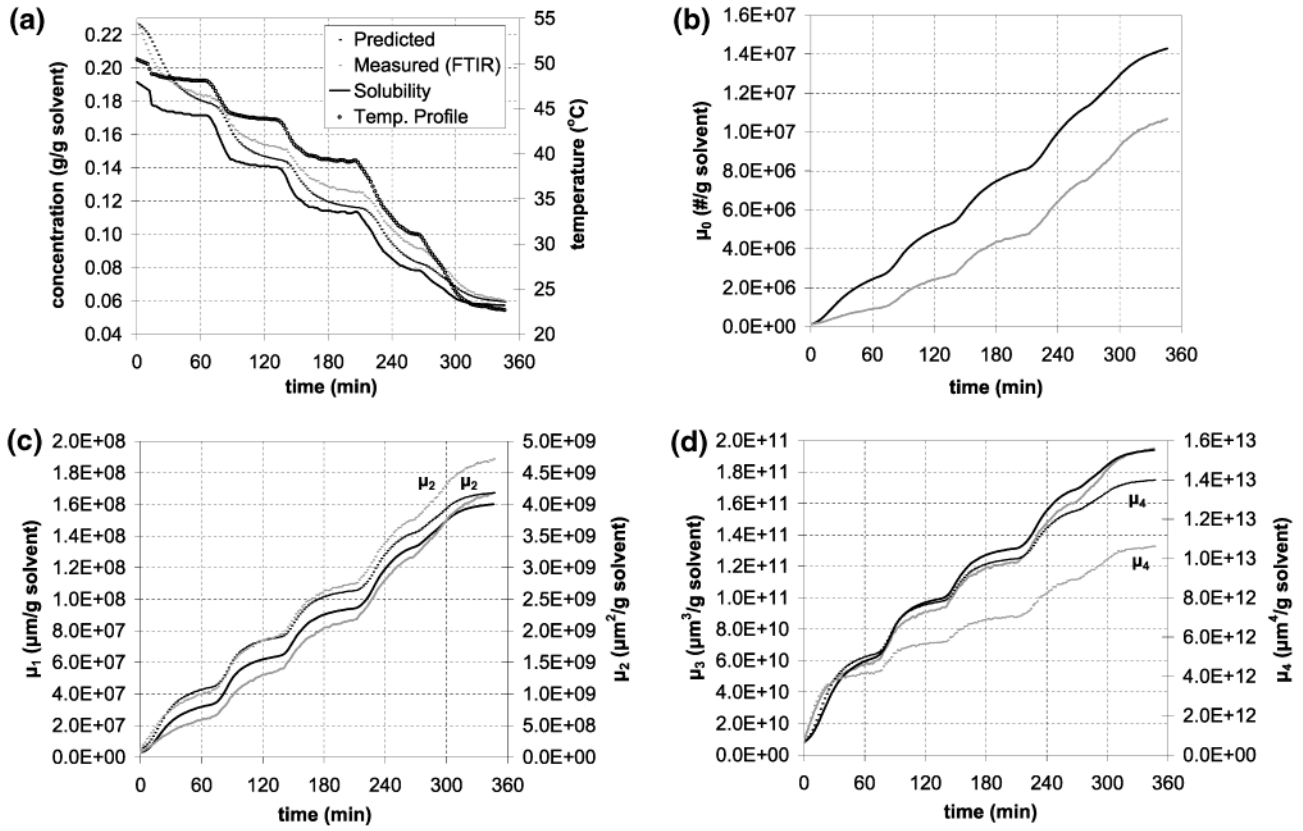

Figure 7. Predicted (black) and measured (gray) variables for experiment E: (a) solute concentration and temperature profile; (b) zeroth moment, μ_0; (c) first moment (solid), μ_1, and second moment (dashed), μ_2; (d) third moment (solid), μ_3, and fourth moment (dashed), μ_4.

Table 7. Moment Ratios[a] Measured Using FBRM and Predicted by the One-Dimensional Model

sample	μ_1/μ_0	μ_2/μ_1	μ_3/μ_2	μ_4/μ_3	μ_2/μ_0	μ_3/μ_0
Measured Using FBRM						
seed point	26.4	43.9	62.5	84.0	1.16×10^3	7.25×10^4
first	26.3	42.5	57.5	72.4	1.12×10^3	6.44×10^4
second	21.2	35.3	48.8	62.1	7.48×10^2	3.65×10^4
third	18.5	31.7	44.8	57.7	5.85×10^2	2.62×10^4
fourth	17.2	30.1	43.0	55.8	5.18×10^2	2.23×10^4
fifth	15.7	28.2	41.3	54.4	4.42×10^2	1.83×10^4
Predicted by the One-Dimensional Model						
seed point	26.4	43.9	62.5	84.0	1.16×10^3	7.25×10^4
first	13.2	33.7	57.2	81.4	4.45×10^2	2.55×10^4
second	12.3	29.8	52.7	78.2	3.67×10^2	1.93×10^4
third	11.7	28.0	50.0	75.8	3.28×10^2	1.64×10^4
fourth	12.0	26.9	48.0	73.9	3.22×10^2	1.55×10^4
fifth	11.2	26.1	46.4	72.0	2.93×10^2	1.36×10^4

[a] The first column is the average crystal length (in μm); the second, third, and fourth columns are the length-weighted, area-weighted, and volume-weighted crystal lengths, respectively (in μm); the fifth column is the average crystal area divided by 9.2 (in μm^2); and the sixth column is the average crystal volume divided by 1.8 (in μm^3).

Table 8. Two-Dimensional Moment Ratios[a] Measured by Off-line Optimal Microscopy and Image Analysis

sample	μ_{10}/μ_{00}	μ_{01}/μ_{00}	μ_{20}/μ_{10}	μ_{02}/μ_{01}	μ_{21}/μ_{11}	μ_{11}/μ_{10}	μ_{11}/μ_{01}
seed	10.2	11.6	20.8	22.3	26.9	22.6	20.0
first	12.5	20.0	28.5	43.6	49.5	40.5	25.5
second	11.3	18.5	27.0	43.1	47.2	38.5	23.4
third	11.9	19.8	29.0	40.6	54.8	41.0	24.6
fourth	11.0	18.3	28.8	41.9	55.8	39.7	23.8
fifth	11.6	19.5	29.6	37.2	63.0	41.0	24.3

[a] The first column is the average width, the second column is the average length, and the remaining columns are average lengths and widths weighted by various combinations of the length and width (in μm).

the samples by the average width and length (μ_{10}/μ_{00} and μ_{01}/μ_{00}) measured by off-line optical microscopy. Except for the first sample, the average size measured by FBRM was fairly close to the average length measured by off-line optical microscopy, and the average size predicted by the one-dimensional model is fairly close to the average width measured by off-line optical microscopy. The weighted lengths and widths share many similar qualitative trends among the three sets of moment ratios.

On the basis of the relatively good agreement between the FBRM data and the CSD measured using off-line microscopy and the relatively good agreement of the kinetic parameters, it is likely that there was a cancellation of errors when the FBRM data were used in the modeling of the loosely bound aggregates. For single particles, the CLD is shifted downward from the PSD,[19,22,23] in which case the moments of the CLD would be smaller than the moments of the PSD. For loosely bound aggregates, the laser beam crosses both individual crystals in the aggregate (as it crosses "fingers" of the aggregates) and multiple crystals when they are sufficiently stuck together. The chord from the individual crystals will typically underestimate the size of the individual crystals, whereas many of the chords obtained when crossing multiple crystals will overestimate the size of individual crystals. The effects tend to compensate each other.

6.6. Considerations on Convergence to a Local Minimum for All Parameter Estimation Runs. For each set of parameter estimation calculations, the gradient vectors of the objective function were computed and found to be very small ($\sim 10^{-5}$–10^{-7} of the objective

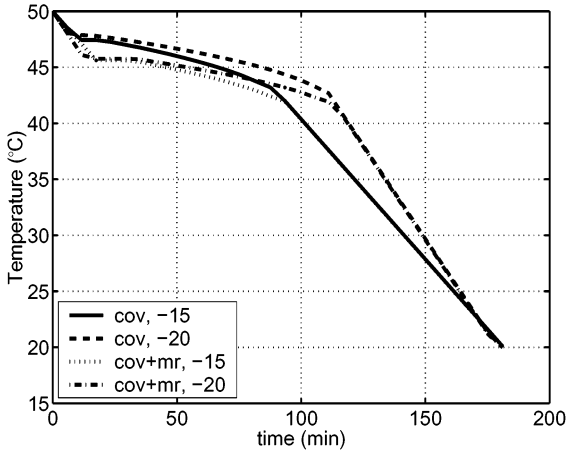

Figure 8. Temperature profiles calculated to minimize (a) the cov (covariance) and (b) the sum of the cov and nucleated-to-seed mass ratio (cov + mr) for the maximum cooling rates of 15 and 20 °C/h.

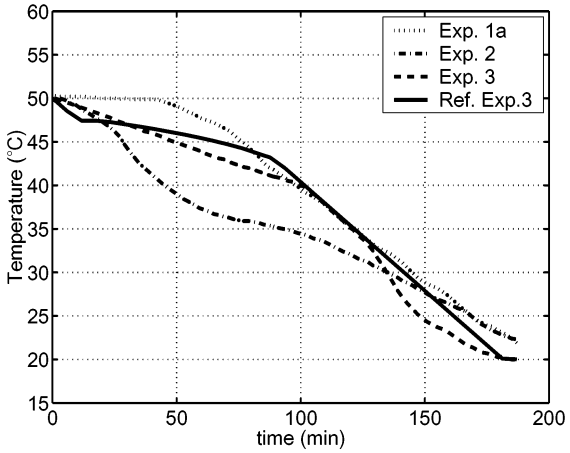

Figure 9. Temperature profiles for experiment 1a (current procedure), experiment 2 (experiment designed to maximize the information content of data), experiment 3 (experiment designed to minimize cov), and the set-point trajectory for experiment 3.

function value) except for the growth exponent g, whose gradient was negative for all sets of parameters for which the growth exponent was equal to its upper bound ($g = 2$). The gradient for the nucleation exponent b was very small for all sets of parameters, even at its lowest value of $b = 1$. This indicates that dropping the lower constraint on the nucleation exponent would have a very small effect on the computed value for b. Within numerical accuracy, these gradients satisfy the first-order necessary conditions for the estimated parameters being located at a (local) minimum.[40] The Hessians were computed for each set of parameters and inserted into the second-order sufficient conditions,[40] which were satisfied for all sets of parameters.

6.7. Optimization of Crystal Properties. Once the kinetic parameters were estimated to sufficiently high accuracy and the model verified in the additional batch experiment, the model was used to compute a temperature profile and seed load that minimizes the cov, or a weighted sum of the cov and the nucleated-to-seed mass ratio. The seed load for the optimized operating procedures was at its maximum allowed value (6%, see Table 2). This result is consistent with past simulation and experimental studies that found the maximum seed load to be optimal for a wide range of operating regimes[1] and crystal−solvent combinations (see ref 10 and references therein).

Temperature profiles were designed for each of the optimization objectives for a temperature profile consisting of either 16 or 32 linear segments, a maximum cooling rate of 15 or 20 °C/h, and a maximum heating rate of 0, 15, or 20 °C/h (see Figure 8). The cov, the nucleated-to-seed mass ratio, and their sum are reported in Table 9 for the case in which the objective to be minimized is the cov and for the case in which the objective to be minimized is the sum of the cov and the nucleated-to-seed mass ratio. Increasing the linear segments from 16 to 32 gave a minor improvement in either objective function. Allowing a positive upper bound on the temperature gradient did not provide significant improvement in the objective function values for either optimization problem. It is conjectured that short bursts of heating[41] would have a greater effect for crystals having dissolution kinetics that are much faster than the growth kinetics, as this would provide greater asymmetry between the effects of heating and cooling. Also, heating is more likely to provide improved product quality if the batch time is long, as short batch times and physical constraints on the heating and cooling rates can limit the amount of heating that can be carried out during the batch while satisfying the constraint on the yield of crystals at the end of the batch.[41] Any improvement provided by heating would have to be rather significant to justify the increased energy costs. In contrast, increasing the maximum cooling rate by 5 °C/h (from 15 to 20 °C/h) would not significantly affect the energy costs and improved the cov and the sum of cov and nucleated-to-seed mass ratio.

The temperature profile for minimization of the cov and nucleated-to-seed mass ratio drops more quickly for the first 50 min than for minimization of cov only, reducing the mass ratio by 8−14% (as shown in Table 9). The temperature profile for minimization of the cov was implemented experimentally (see Figure 9). The temperature was not very well controlled in the crystallizer, which simulates the effect of spatial variations

Table 9. Coefficient of Variation (cov), Nucleated-to-Seed Mass Ratio (mr), and Their Sum from Numerical Simulation to Minimize (a) cov and (b) the Sum of cov and the Nucleated-to-Seed Mass Ratio (cov + mr) for Varying Number of Linear Segments, Maximum Rate of Cooling, and Maximum Rate of Heating

number of segments	temperature gradient (°C/h)		minimum cov			minimum cov + mr		
	minimum	maximum	cov	mr	cov + mr	cov	mr	cov + mr
16	−15	0	1.151	0.228	1.379	1.161	0.209	1.370
16	−15	15	1.150	0.228	1.378	1.162	0.208	1.370
32	−15	0	1.144	0.232	1.376	1.155	0.209	1.363
32	−15	15	1.144	0.232	1.376	1.154	0.209	1.363
16	−20	0	1.094	0.244	1.338	1.107	0.211	1.318
16	−20	20	1.094	0.244	1.338	1.107	0.211	1.318
32	−20	0	1.088	0.246	1.334	1.104	0.211	1.315
32	−20	20	1.088	0.246	1.334	1.105	0.209	1.314

Table 10. Computed Coefficient of Variation (cov) and Nucleated-to-Seed Mass Ratio (mr) for the Current Procedure, the Modified Current Procedure (Same Temperature Profile, Double the Amount of Seed), the Designed Experiment for Parameter Estimation, and the Optimized Experiment That Minimizes cov[a]

experiment	cov	mr
current procedure (Table 2, expt 1a)	1.24	0.61
modified current procedure	1.23	0.26
designed experiment (Table 2, expt 2)	1.36	0.94
minimize cov (Table 2, expt 3)	1.16	0.38

[a] The seed load was 3% for experiments 1a and 2 and 6% for experiment 3 and the modified current procedure.

and the effects of other disturbances in industrial-scale crystallizers. Such disturbances motivate the definition of a modified current procedure, which has the same temperature profile as experiment 1a, but with twice the seed load. The motivation behind defining the modified current procedure is to test whether most of the improvement in product quality is due to the increased seed load rather than the improved temperature profile.

Four batch runs were simulated with various temperature profiles and seed loads (see Table 10). The impact of seed mass on the nucleated-to-seed mass ratio is profound (compare rows 1 and 2 in Table 10). The effect of the temperature profile is significant for both objectives (compare rows 2 and 4 in Table 10). The modified current procedure has a somewhat larger cov and a much smaller nucleated-to-seed mass ratio than the operating procedure designed to minimize the cov. Hence, most of the benefit of optimization is due to optimizing the seed load.

The experiment designed to generate data for accurate parameter estimation produced conditions resulting in a very high nucleated-to-seed mass ratio and cov. This is also not surprising given that the experiment was designed to produce high information content in the data, which, in this case, meant creating conditions of high supersaturation and nucleation, presumably to provide information on the nucleation kinetics.

6.8. Predictions and Measurements for the Optimized Experiment. The predicted and measured solute concentration and the low-order moments are reported for the experiment designed by minimizing the cov (see Figure 10). There is some overprediction of the solute concentration for the initial half of the crystallization procedure and some underprediction of the solute concentration for the second half. Good agreement is established for the solute concentration in the last half of the run and the first, second, and third moments for the entire run. The agreement is poorer for the zeroth and fourth moments, which is not surprising, as discussed previously.

7. Conclusions

Model-based experimental design and parameter estimation, coupled with in situ infrared and laser backscattering instrumentation, was applied to the cooling crystallization of a drug compound to construct a model for use in the design of an optimal operating procedure. After two batch experiments, the method improved the confidence levels of the nucleation and growth rate parameters by 2−3 times to a precision of <12%. Modeling issues involving the selection of the expressions for the supersaturation and nucleation rate, as well as the electronics mode in the FBRM instrument, were explored. The absolute supersaturation expression gave smaller confidence intervals on the

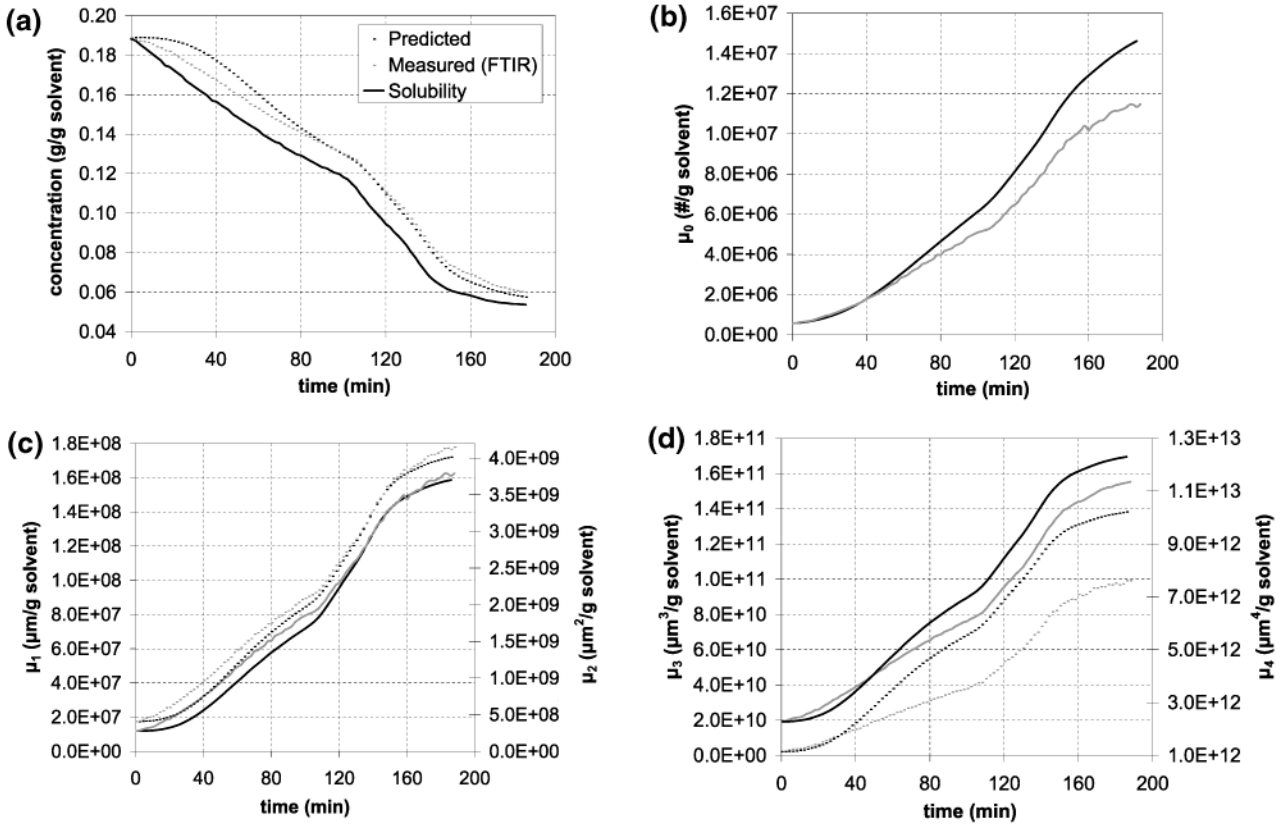

Figure 10. Predicted (black) and measured (gray) variables for experiment 3: (a) solute concentration; (b) zeroth moment, μ_0; (c) first moment (solid), μ_1, and second moment (dashed), μ_2; (d) third moment (solid), μ_3, and fourth moment (dashed), μ_4.

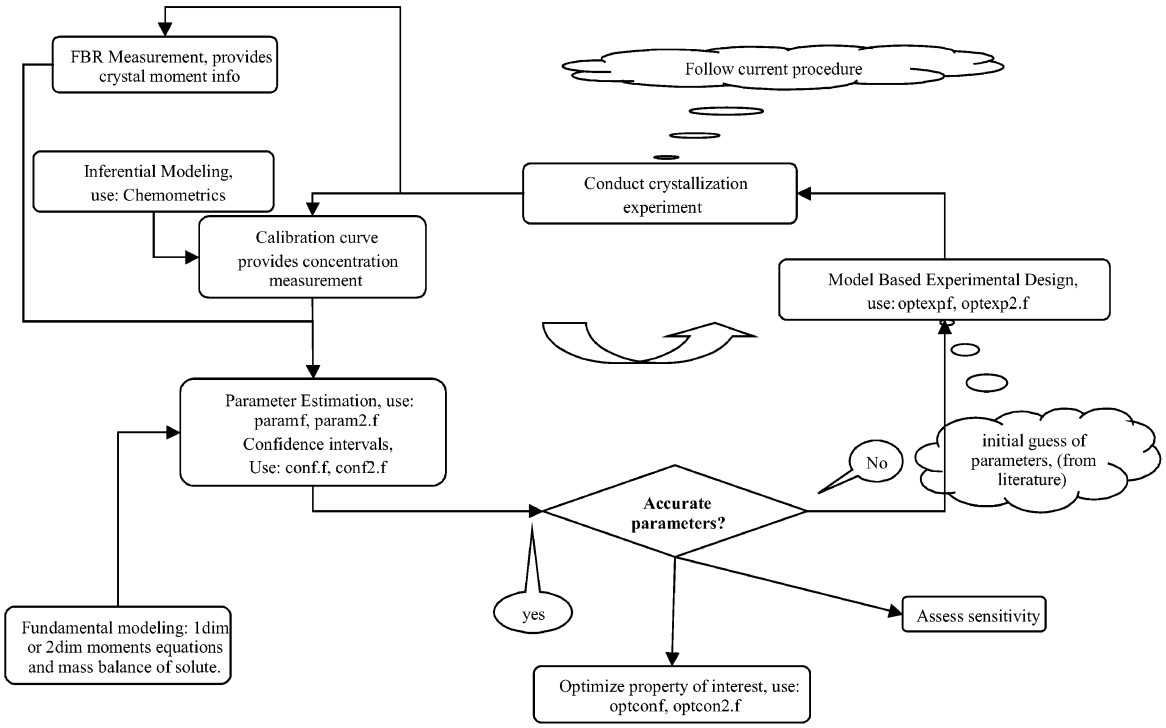

Figure 11. Diagram of the overall procedure used in the present study, including software information.

parameters than relative supersaturation, and the "fine" electronics mode in the FBRM gave smaller confidence intervals than the "coarse" mode. Choice of the nucleation rate expression did not significantly influence the size of the confidence intervals. The model produced acceptable predictions in an independent evaluation experiment, where it was found that almost all of the kinetic parameters were close to parameters identified using off-line particle size measurement. These parameters were used to optimize the crystallization process by maximizing crystal growth and minimizing a measure of the width of the particle size distribution (the coefficient of variation).

Acknowledgment

The authors thank Terry Redman of Mettler-Toledo for comments on the manuscript.

Appendix

The diagram for the overall procedure along with the software that was used at each step is shown in Figure 11. The FORTRAN codes are available on the Internet.[42] The codes are as follows: (i) dim1.f/dim2.f simulates a 1D/2D batch crystallizer, (ii) param.f/param2.f estimates the nucleation and growth kinetic parameters for a 1D/2D batch crystallizer, (iii) conf.f/conf2.f computes the confidence intervals on the nucleation and growth kinetic parameters, (iv) optexp.f/optexp2.f computes the model-based experimental design, and (v) optcon.f/optcon2.f computes the operating procedure for a product with optimized properties.

There are PC and Sun versions of the FORTRAN codes, which use the IMSL libraries. For inferential modeling, the Robust Chemometrics Toolbox was used and is available to restricted parties. The software that came with the FBRM instrument was used to measure the CLD. The chord length number distribution was used, which collects the number of chords measured into 250 channels with measurements from 0.5 to 500 μm. Numerical integration (summation) was used to calculate the moments from the FBRM data

$$\mu_j = \sum_{k=0}^{k=N-1} \left(\frac{L_k + L_{k+1}}{2}\right)^j \frac{F(L_{k+1},t)}{L_{k+1} - L_k}(L_{k+1} - L_k)$$

$$= \sum_{k=0}^{k=N-1} \left(\frac{L_k + L_{k+1}}{2}\right)^j F(L_{k+1},t)$$

where $F(L_{k+1},t)$ is the number of particles with chord lengths up to L_{k+1} per unit mass solvent at a point in time t, L_0 is the smallest chord length, and L_N is the largest chord length.

Literature Cited

(1) Chung, S. H.; Ma, D. L.; Braatz, R. D. Optimal Seeding in Batch Crystallization. *Can. J. Chem. Eng.* **1999**, *77*, 590−596.

(2) Chung, S. H.; Ma, D. L.; Braatz, R. D. Optimal Model-based Experimental Design in Batch Crystallization. *Chemom. Intell. Lab. Syst.* **2000**, *50*, 83−90.

(3) Matthews, H. B., III. Model Identification and Control of Batch Crystallization for an Industrial Chemical System. Ph.D. Thesis, University of Wisconsin, Madison, Wisconsin, 1997.

(4) Miller, S. M.; Rawlings, J. B. Model Identification and Control Strategies for Batch Cooling Crystallizers. *AIChE J.* **1994**, *40*, 1312−1327.

(5) Braatz, R. D. Advanced Control of Crystallization Processes. *Annu. Rev. Control* **2002**, *26*, 87−99.

(6) Togkalidou, T.; Fujiwara, M.; Patel, S.; Braatz, R. D. Solution Concentration Prediction Using Chemometrics and ATR-FTIR Spectroscopy. *J. Cryst. Growth* **2001**, *231*, 534−543.

(7) Rawlings, J. B.; Miller, S. M.; Witkowski, W. R. Model Identification and Control of Solution Crystallization Processes: A Review. *Ind. Eng. Chem. Res.* **1993**, *32*, 1275−1296.

(8) Hulburt, H. M.; Katz, S. Some Problems in Particle Technology. *Chem. Eng. Sci.* **1964**, *19*, 555−574.

(9) Randolph, A.; Larson, M. A. *Theory of Particulate Processes*, 2nd ed.; Academic Press: San Diego, 1988.

(10) Kubota, N.; Doki, N.; Yokota, M.; Jagadesh, D. Seeding Effect on Product Crystal Size in Batch Crystallization. *J. Chem. Eng. Jpn.* **2002**, *35*, 1063−1071.

(11) Ma, D. L.; Tafti, D. K.; Braatz, R. D. High-Resolution Simulation of Multidimensional Crystal Growth. *Comput. Chem. Eng.* **2002**, *41*, 6217−6223.

(12) Youngquist, G. R., Ed. *Advances in Crystallization from Solutions*; AIChE: New York, 1984, Vol. 80.

(13) Becker, R. A Brief Introduction to Lasentec FBRM. Manufacturer's documentation obtained at the Lasentec User's Forum, New York, New York, February 25−26, 2003.

(14) Wang, S.; Mersmann, A. Size-Dependent Growth-Rate Disperson of Attrition Fragments and Secondary Nuclei. *Chem. Eng. Sci.* **1992**, *47*, 1365−1371.

(15) Beck, J. V.; Arnold, K. J. *Parameter Estimation in Engineering and Science*; Wiley: New York, 1977.

(16) Togkalidou, T.; Braatz, R. D.; Johnson, B.; Davidson, O.; Andrews, A. Experimental Design and Inferential Modeling in Pharmaceutical Crystallization. *AIChE J.* **2001**, *47*, 160−168.

(17) Togkalidou, T.; Fujiwara, M.; Patel, S.; Braatz, R. D. A Robust Chemometrics Approach to Inferential Estimation of Supersaturation. In *Proceedings of the American Control Conference*; IEEE Press: Piscataway, NJ, 2000; pp 1732−1736.

(18) Togkalidou, T.; Tung, H.-H.; Sun, Y.; Andrews, A.; Braatz, R. D. Solution Concentration Prediction for Pharmaceutical Crystallization Processes using Robust Chemometrics and ATR FTIR Spectroscopy. *Org. Process Res. Dev.* **2002**, *6*, 317−322.

(19) Tadayyon, A.; Rohani, S. Determination of Particle Size Distribution By Par-Tec 100: Modeling and Experimental Results. *Part. Part. Syst. Charact.* **1998**, *15*, 127−135.

(20) Richmond, W. R.; Jones, R. L.; Fawell, P. D. The Relationship Between Particle Aggregation and Rheology in Mixed Silica−Titania Suspensions. *Chem. Eng. J.* **1998**, *71*, 67−75.

(21) Lumpe, C. J.; Homburg, L.; Verstraeten, K. Focused Beam Reflectance Measurement (FBRM): A Promising Tool for Wet-end Optimisation and web Break Prediction. *Pap. Technol. Ind.* **2001**, *42*, 39−44.

(22) Ruf, A.; Worlitschek, J.; Mazzotti, M. Modeling and Experimental Analysis of PSD Measurements through FBRM. *Part. Part. Syst. Charact.* **2000**, *17*, 167−179.

(23) Hukkanen, E. J.; Braatz, R. D. Measurement of Particle Size Distribution in Suspension Polymerization using in situ Laser Backscattering. *Sens. Actuators B* **2003**, *96*, 451−459.

(24) Simmons, M. J. H.; Langston, P. A.; Burbidge, A. S. Particle and Droplet Size Analysis from Chord Distributions. *Powder Technol.* **1999**, *102*, 75−83.

(25) Heath, A. R.; Fawell, P. D.; Bahri, P. A.; Swift, J. D. Estimating Average Particle Size by Focused Beam Reflectance Measurement (FBRM). *Part. Part. Syst. Charact.* **2002**, *195*, 84−95.

(26) Ljung, L. *System Identification: Theory for the User*; Prentice-Hall: Englewood Cliffs, NJ, 1987.

(27) Atkinson, A. C.; Donev, A. N. *Optimum Experimental Designs*; Oxford University Press: New York, 1992.

(28) Box, G. E.; Lucas, H. L. Design of Experiments in Nonlinear Situations. *Biometrica* **1959**, *46*, 77−90.

(29) Espie, D.; Macchietto, S. The Optimal Design of Dynamic Experiments. *AIChE J.* **1989**, *35*, 223−229.

(30) David, R.; Villermaux, J.; Marchal, P.; Klein, J. P. Crystallization and Precipitation Engineering 4. Kinetic Model of Adipic Acid Crystallization. *Chem. Eng. Sci.* **1991**, *46*, 1129−1136.

(31) Jager, J.; de Wolf, S.; Kramer, H.; de Jong, E. J. Estimation of Nucleation and Attrition Kinetics from Crystal Size Distribution Transients in a Continuous Crystallizer. *Trans. Inst. Chem. Eng* **1991**, *69*, 53−62.

(32) Palwe, B.; Chivate, M.; Tavare, N. S. Growth Kinetics of Ammonium Nitrate Crystals in a Draft Tube Baffled Batch Crystallizer. *Ind. Eng. Chem. Process Des. Dev.* **1985**, *24*, 914−919.

(33) Tavare, N. S. Batch Crystallizers: A Review. *Chem. Eng. Commun.* **1987**, *61*, 259−318.

(34) Witkowski, W. R.; Miller, S. M.; Rawlings, J. Light-Scattering Measurements to Estimate Kinetic Parameters for Crystallization. *ACS Symp. Ser.* **1990**, *438*, 102−114.

(35) Gunawan, R.; Ma, D. L.; Fujiwara, M.; Braatz, R. D. Identification of Kinetic Parameters in Multidimensional Crystallization Processes. *Int. J. Mod. Phys. B* **2002**, *16*, 367−374.

(36) Rawlings, J. B.; Sink, C. W.; Miller, S. M. Control of Crystallization Processes. In *Handbook of Industrial Crystallization*; Myerson, A. S., Ed.; Butterworth-Heinemann: Boston, MA, 1993; pp 179−207.

(37) Fletcher, R. *Practical Methods of Optimization*, 2nd ed.; John Wiley & Sons, Inc.: New York, 1987.

(38) Zhou, J. L.; Tits, A. L. *FSQP*; AEM Design: Tucker, GA, 1989 (available at http://64.238.116.66/aemdesign/FSQPframe.htm).

(39) Ohara, M.; Reid, R. C. *Modeling Crystal Growth Rates from Solution*; Prentice Hall: Englewood Cliffs, NJ, 1979.

(40) Luenberger, D. G. *Linear and Nonlinear Programming*, 2nd ed.; Addison-Wesley: Reading, MA, 1984.

(41) Takiyama, H.; Shindo, K.; Matsuoka, M. Effects of Undersaturation on Crystal Size Distribution in Cooling Type Batch Crystallization. *J. Chem. Eng. Jpn.* **2002**, *35*, 1072−1077.

(42) Chung, S. H.; Ma, D. L.; Fujiwara, M.; Gunawan, R.; Togkalidou, T.; Braatz, R. D. *Simulation, Parameter Estimation, Experimental Design, and Optimal Control of Batch Crystallization*; University of Illinois: Urbana, IL, 1999 (available at http://brahms.scs.uiuc.edu/lssrl/software/crystal).

Received for review August 21, 2003
Revised manuscript received February 10, 2004
Accepted June 30, 2004

IE0340847